J. Phys. D: Appl. Phys. **41** (2008) 194009 (6pp) doi:10.1088/0022-3727/41/19/194009

On-chip microplasma reactors using carbon nanofibres and tungsten oxide nanowires as electrodes

Anil Ağiral[1], Alfons W Groenland[1], J Kumar Chinthaginjala[2], K Seshan[2], Leon Lefferts[2] and J G E Han Gardeniers[1]

[1] Mesoscale Chemical Systems, MESA+ Institute for Nanotechnology, University of Twente, PO Box 217, 7500 AE, Enschede, The Netherlands
[2] Catalytic Processes and Materials, MESA+ Institute for Nanotechnology, University of Twente, PO Box 217, 7500 AE, Enschede, The Netherlands

E-mail: a.agiral@utwente.nl

Received 21 January 2008, in final form 11 May 2008
Published 15 September 2008
Online at stacks.iop.org/JPhysD/41/194009

Abstract
Carbon nanofibres (CNFs) and tungsten oxide ($W_{18}O_{49}$) nanowires have been incorporated into a continuous flow type microplasma reactor to increase the reactivity and efficiency of the barrier discharge at atmospheric pressure. CNFs and tungsten oxide nanowires were characterized by high-resolution scanning electron microscopy, transmission electron microscopy and nanodiffraction methods. Field emission of electrons from those nanostructures supplies free electrons and ions during microplasma production. Reduction in breakdown voltage, higher number of microdischarges and higher energy deposition were observed at the same applied voltage when compared with plane electrodes at atmospheric pressure in air. Rate coefficients of electron impact reaction channels to decompose CO_2 were calculated and it was shown that CO_2 consumption increased using CNFs compared with plane electrode in the microplasma reactor.

1. Introduction

Miniaturized plasma sources have generated considerable interest recently, owing to a number of important applications [1]. Performing the plasma process in a microreactor leads to precise control of residence time and extreme quenching conditions, enabling control over the reactants to selectively produce desirable products [2].

Carbon nanofibres (CNFs) and $W_{18}O_{49}$ nanowires have remarkable field emission characteristics [3, 4]. Their high aspect ratio structures generate local field enhancement at the apex of nanoscale tip and lower the threshold voltage for field emission and field ionization. Field electron emission and field ionization can supply free electrons and ions which can contribute to pre-breakdown current during the initiation of the discharge. The process of multiplication of electrons in a series of impact ionization can lower the breakdown voltage in microplasma devices. Eden and Park [5] demonstrated that incorporation of multiwall carbon nanotubes (CNTs) into the cathode reduces the ignition voltage and increases the radiative efficiency. From plasma catalysis point of view, field emitted electrons can vibrationally excite the molecules near the surface and activation energy for dissociative adsorption can be lowered [6].

In this work, CNFs and $W_{18}O_{49}$ nanowires were incorporated into silicon chip electrode which was placed in a glass microreactor channel. Characteristics of dielelectric barrier discharge with $W_{18}O_{49}$ nanowires and CO_2 conversion with CNFs and their comparison with plane-to-plane electrodes without nanostructures are discussed.

2. Experimental procedure

2.1. Synthesis of CNFs and $W_{18}O_{49}$ nanowires

For CNFs, the standard (1 0 0) n-type silicon wafers were cleaned in fuming HNO_3 to remove organic and inorganic species. Wafers were patterned in a standard lithography process finishing with 20 min 120 °C postbake. 10 nm nickel catalyst and 10 nm tantalum barrier layers were deposited by

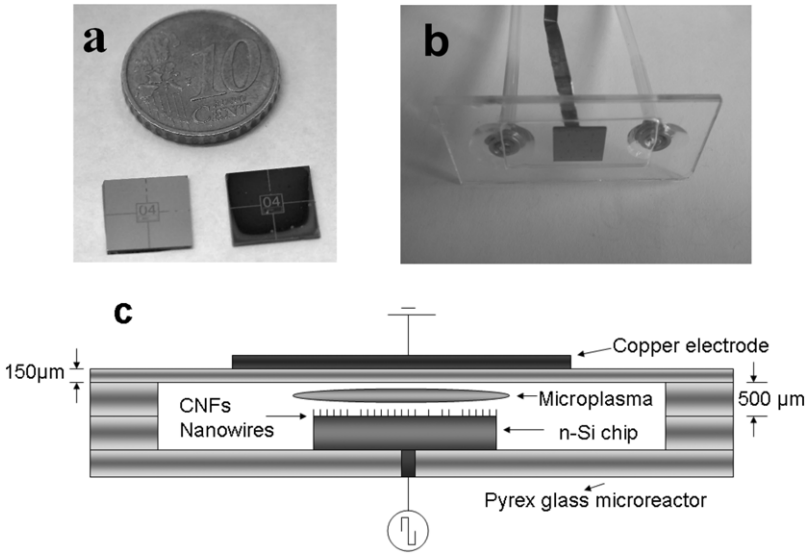

Figure 1. (*a*) Silicon chip before and after CVD process, (*b*) microplasma reactor and (*c*) the general diagram of the device.

electron beam evaporation. Excess metal was removed by lift-off in acetone, enhanced by ultrasonic agitation. Samples with regular arrays of metal dots with 4 μm in diameter were fabricated. For $W_{18}O_{49}$ nanowires, 250 nm titanium–tungsten alloy and 50 nm tungsten metal layers were deposited by plasma sputtering. Silicon chips with Ni and W layers were placed in a chemical vapour deposition (CVD) setup. Tungsten oxide nanowires and CNFs were grown on tungsten and nickel thin films respectively, which were exposed to 27 sccm of C_2H_4 and 80 sccm of N_2 at 700 °C at atmospheric pressure for 20 min. In figure 1(*a*), two silicon chips are shown. The black one (on the right) represents the situation after CNFs growth and the chip shown on the left indicates the sample before the growth of the CNFs.

2.2. Microplasma reactor and experimental setup

Silicon chips were placed in glass microreactors. The rectangular cross section of microreactor is 50 mm in length and 20 mm in width. Microchannels, inlet and outlet holes for gas flow were created by powder blasting and glass layers were thermally bonded to seal the microchannel hermetically. The real picture and the representation of the device are shown in figures 1(*b*) and (*c*), respectively.

The field emission characterization system employs CNFs or $W_{18}O_{49}$ nanowires on silicon substrates as cathodes and the n-type silicon chip electrode as anode at atmospheric pressure in air. 2 μm thick SiO_2 spacer layer was grown by wet oxidation on the anode and a rectangular window with 0.7 cm^2 area was removed by etching with BHF solution. The anode chip mounted faced down to ensure a 2 μm electrode distance to analyse field emission from nanostructures at atmospheric pressure. A Keithley 237 sourcemeter unit was used to record *I*–*V* curves.

Combination of a high voltage amplifier (Trek 610E) and a function generator (Agilent 3322A) was used to generate barrier discharge in microplasma reactor at 1 kHz. Voltage drops across a resistor and a capacitor connected in series with reactor were used to calculate transferred current and charge, respectively. Light emitted from the barrier discharge was collected by inserting an optical fibre to the microchannel and optical emission spectrometer (HR 4000, Ocean Optics) was used for obtaining spectra. Power absorbed by the plasma was evaluated on the basis of a Lissajous figure measured with an oscilloscope.

Experimental apparatus for testing CO_2 decomposition to CO and O_2 using CNFs as electrodes consists of mass flow controllers and mass spectrometer. The gas flow was controlled by mass flow controllers. CO_2 flows through the inlet of the microreactor and processed in the barrier discharge region between the silicon chip with nanostructures and the glass dielectric. A quadrupole ion-trap mass spectrometer (Pfeiffer QMS 422) with residual gas analyzer was used for gas analysis. Helium gas with a known flow rate was mixed with CO_2 before introducing to the reactor. Mole fractions of gases were measured in the previously calibrated mass spectrometer. Conversion of CO_2 was calculated on the basis of the known flow rate of He and mole fraction of unreacted CO_2.

3. Results and discussion

3.1. Characterization of CNFs and tungsten oxide nanowires

Figure 2(*a*) shows the arrays of dots where CNFs were successfully grown on nickel layers with CVD process. Very dense CNFs were grown on the chip with a maximum height around 2–3 μm. Higher aspect ratio structures in the random arrangement of nanofibres have the maximum probability for field emission due to their higher field amplification factor. Figure 2(*b*) shows a single dot with 4 μm diameter.

Figures 3(*a*) and (*b*) show high-resolution scanning electron microscopy (HR-SEM) images of the sample depicting morphology of tungsten oxide nanowires grown on tungsten film on silicon substrate. Highly dense nanowires were obtained. These nanowires are uniform in diameter, ranging from 10 to 20 nm and up to 400 nm in length.

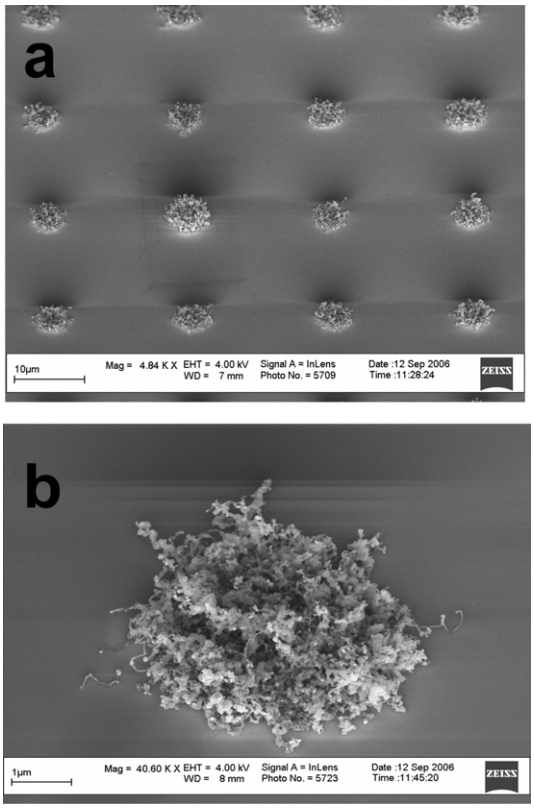

Figure 2. HR-SEM images of CNFs growth experiment at 700 °C for 20 min showing (*a*) arrays and (*b*) a single dot of 4 μm.

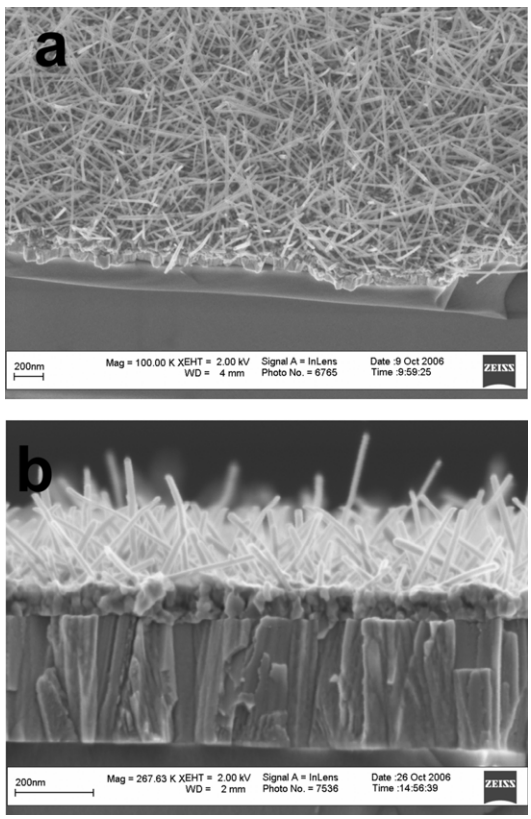

Figure 3. HR-SEM images of tungsten oxide nanowires growth experiment at 700 °C for 20 min showing (*a*) surface of the film and (*b*) the cross section.

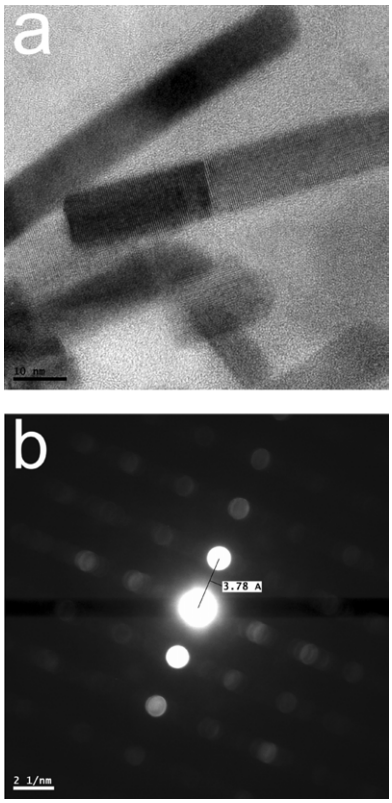

Figure 4. (*a*) HR-TEM image of tungsten oxide nanowires growth experiment at 700 °C for 20 min and (*b*) nanodiffraction analysis showing the strong diffraction spot along the long length of the nanowire.

Tungsten oxide nanowires were further characterized by high-resolution transmission electron microscopy (HR-TEM) (figure 4(*a*)), x-ray photo electron spectroscopy (XPS) and energy dispersive x-ray (EDX) analysis. d-spacing as derived from high-resolution TEM lattice images (3.78 $\pm$ 0.04 Å) is in agreement with the nanodiffraction analysis showing the strong diffraction spot along the long length of the nanowire as shown in figure 4(*b*). This corresponds to the [0 1 0] plane of monoclinic $W_{18}O_{49}$ and from the nanodiffraction pattern, [0 1 0] is confirmed as the major growth direction of nanowires. The EDX analysis confirmed that oxygen is in the order of 2.73 times the amount of tungsten. Investigation of the chemical bonding states on the surface of the tungsten thin film and nanowires indicated that the intensity ratio of binding states of oxidized tungsten to metallic tungsten increased as it is consistent with $W_{18}O_{49}$ nanowire formation. Details of the synthesis and growth mechanism of the nanowires will be published elsewhere.

3.2. Tungsten oxide nanowires as microplasma electrodes at atmospheric pressure in air

The *I*–*E* characteristics of field emission experiments with tungsten oxide nanowires and CNFs are shown in figure 5(*a*). The leakage current which arises from the conduction along the 2 μm thickness SiO_2 spacer in the field emission diode system was determined by measuring the current between n-type silicon electrodes separated by 2 μm thickness SiO_2 layer

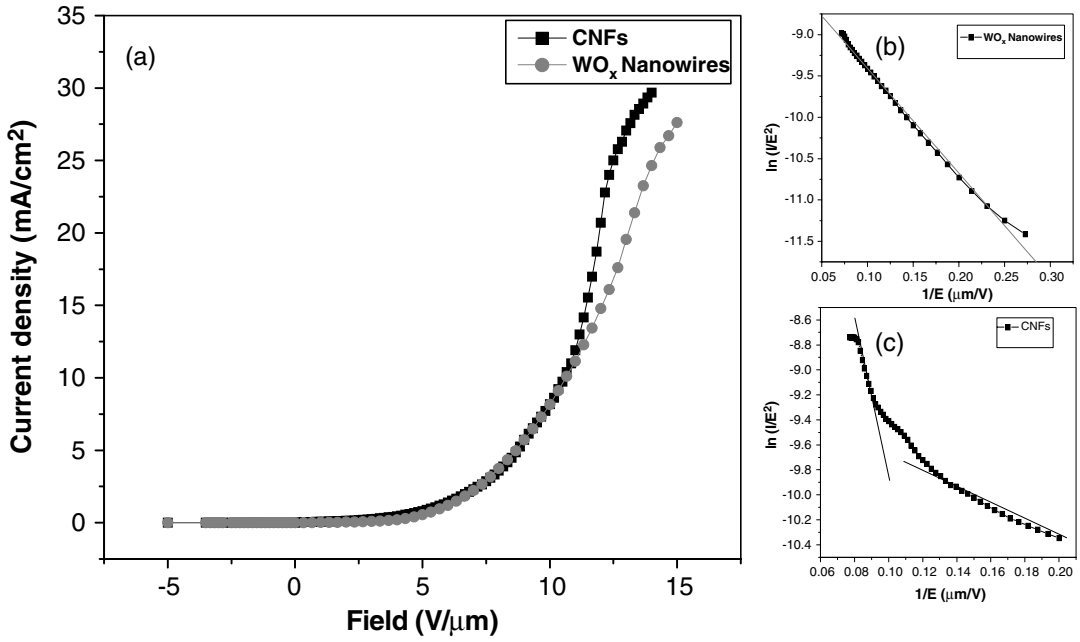

Figure 5. (*a*) I–E characteristics of CNFs and tungsten oxide nanowires in a field emission diode system in 2 μm gap at atmospheric pressure in air, and F–N plots [$\ln(I/E^2)$ versus E^{-1}] of I–E characteristics of (*b*) nanowires and (*c*) nanofibres.

by applying 30 V potential. This leakage current remained 7 nA. The field emission current is significantly greater than the leakage current which is negligible. The extractor turn-on field is around 5 V μm^{-1} for both nanowires and CNFs. Exponentially rising current indicates the electron tunnelling from the tips of nanostructures due to enhancement of electric field. CNFs revealed higher electron emission current in the 11 and 13 V μm^{-1} region. Furthermore, Fowler–Nordheim (F–N) plots are shown in figures 5(*b*) and (*c*) for nanowires and nanofibres, respectively. Linear relationship in the F–N plot [$\ln(I/E^2)$ versus E^{-1}] suggests the electron tunnelling. The F–N plot for CNFs have two slopes at lower and higher fields, which shows the contribution of different electron emission sites. At higher electric fields (>13 V μm^{-1}), field emission current enters a saturation region.

The silicon chip containing nanowires was incorporated in a glass microchannel to generate barrier discharge between nanowires and copper tape electrode protected by a glass dielectric (thickness of glass is 150 μm and channel depth is 500 μm). Square wave voltage with 1 kHz frequency was applied to the silicon chip while the copper tape is grounded. Figure 6 shows the measured discharge current spikes in air at atmospheric pressure to compare tungsten oxide nanowires and tungsten film electrode. The breakdown voltage during barrier discharge generation was defined by voltage level where the light emission was detected by optical emission spectrometer with acquisition time of 0.1 s. The current transferred during the streamers production shows a sudden increase due to the breakdown of the gas gap. This breakdown voltage reduced from 4800 to 3720 V in the case of nanowires. This clearly shows that microdischarges started to occur at lower voltages due to electric field enhancement on nanowire electrode. The amount of current that is transferred across the gap is also much higher in the case of nanowires electrode. Reduction

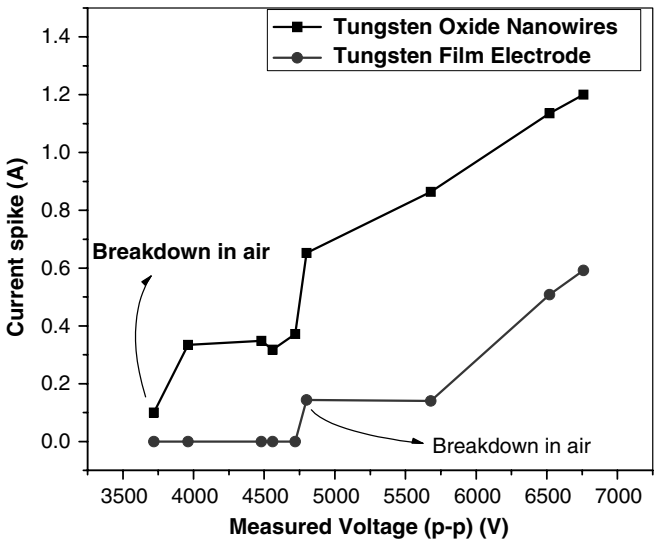

Figure 6. Comparison of discharge current spikes measured in tungsten oxide nanowires and plane tungsten film electrode with varying applied voltage (peak-to-peak), $f = 1$ kHz.

of breakdown voltage and increase in transferred current are suggestive of electric field amplification and emission of electrons on the nanowires surface. Electric field inside the microplasma reactor (5 V μm^{-1}) is enough to generate field emitted electrons before breakdown. Since there is a native oxide layer with a thickness of a few nanometres on the tungsten film, it is believed that both electrode surfaces have similar work functions.

Figure 7 shows the comparison of deposited power into the microplasma as a function of measured voltage. Higher energy density microplasma was obtained with nanowires electrodes at the same voltage due to the generation of a higher number of microdischarges compared with a plane tungsten film. Local

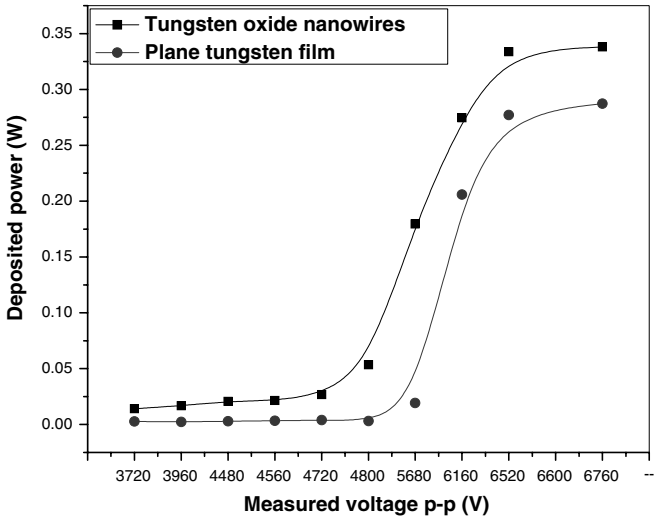

Figure 7. Comparison of deposited power into microplasma measured in tungsten oxide nanowires and plane tungsten film electrode with varying applied voltage (peak-to-peak), $f = 1$ kHz.

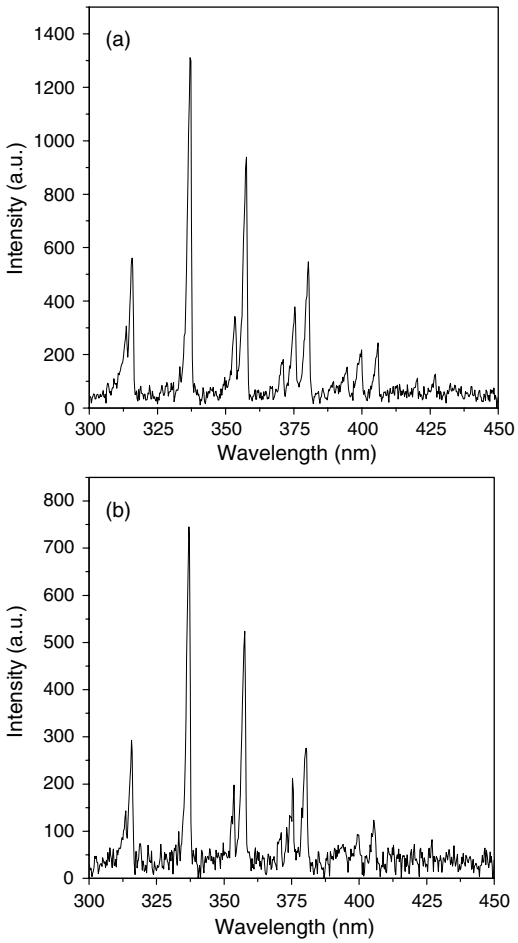

Figure 8. Emission spectra of the microplasma generated using (*a*) tungsten oxide nanowires and (*b*) tungsten film plane electrodes at atmospheric pressure in air, V: 6770 p-p square wave voltage at 1 kHz frequency.

electric field enhancement on the surface helped to increase the number of microdischarges. Microplasma volume also increased since more streamers were generated and discharge became homogeneous. An optical fibre was inserted into

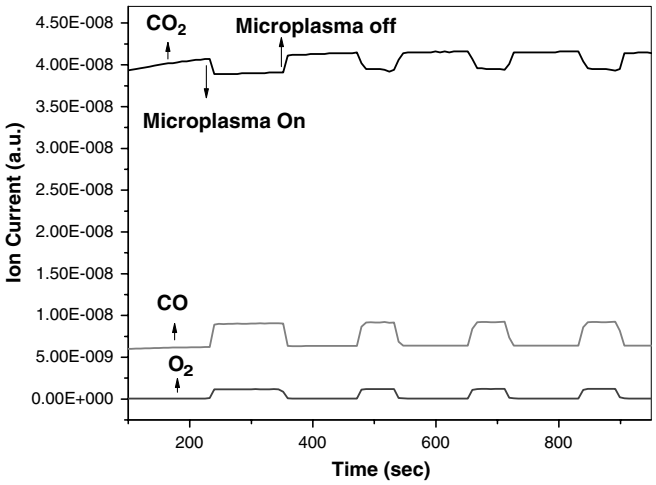

Figure 9. Mass spectrometric analysis of CO_2 conversion in microplasma reactor with CNFs electrodes at 10 sccm, $f = 1$ kHz, measured voltage 5.5 kV (p-p).

microchannel to analyse the light emission. Observed spectra are shown in figure 8(*a*) for tungsten oxide nanowires and in figure 8(*b*) for plane tungsten film electrodes. In the case of nanowires, intensity of the emission lines is much higher. Jani *et al* [7] investigated the variation of electron temperature by spectroscopic measurement using the second positive system (SPS) of N_2 (337.1 nm) and the first negative system (FNS) of N_2^+ (391.4 nm). They showed that the ratio of the SPS to the FNS changes according to the electron temperature in the discharge and intensity ratios of these lines (FNS of N_2^+/SPS of N_2) increase with increasing average electron energy. Intensity ratios were calculated as 0.061 and 0.058 for nanowires and plane electrodes, respectively. There is no remarkable difference although the intensity of the emission lines is much higher for the spectrum of nanowires electrode at the same applied voltage.

3.3. CO_2 consumption in the microplasma reactor with CNFs as electrodes at atmospheric pressure

Carbon dioxide conversion to carbon monoxide and oxygen is an endothermic reaction with an enthalpy of 283 kJ mol^{-1}. This reaction can be used to dispose carbon dioxide or to produce oxygen. The arrays of CNFs grown on the silicon chip were used to compare the conversion levels with plane electrode at the same applied potential. Electrical characterization of the plasma showed that CNFs electrodes generated more microdischarges than the plane electrodes and energy density deposited into the microplasma also increased. Helium was introduced to a reactor with 10 sccm flow rate and mole fraction data were obtained by a mass spectrometry analysis. The conversion of CO_2 was calculated based on the calibrated ion current data which lead to calculation of mole fractions and CO_2 flow before and after the microplasma processing. As the plasma ignited, O_2 and CO formation were observed in the spectrum as shown in figure 9. Since gas temperature in the microplasma is ambient, there is no thermal cracking in the microreactor. Inelastic electron collisions, three body reactions and surface reactions are responsible for

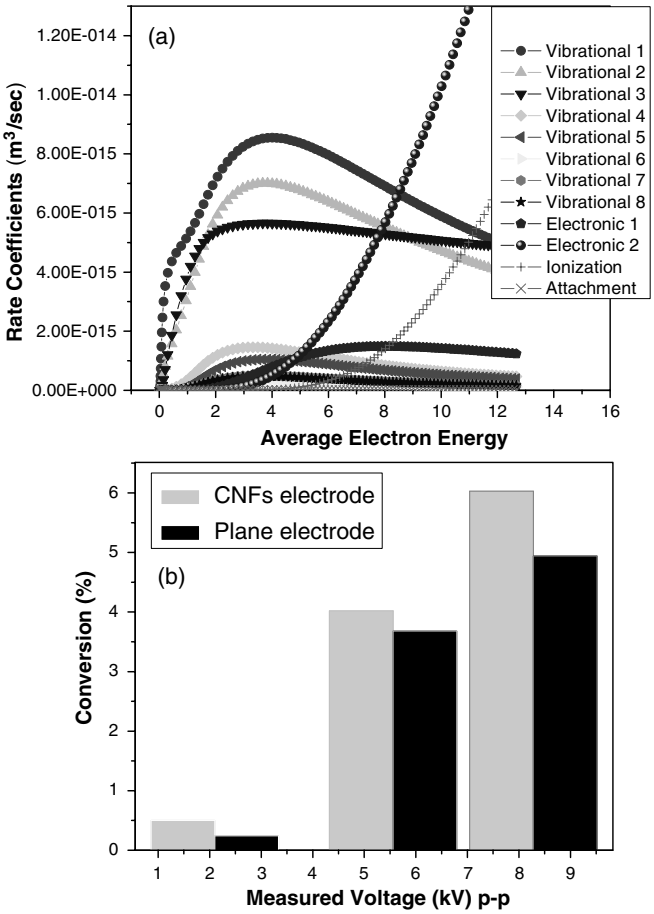

Figure 10. (*a*) Rate coefficients calculated as a function of electron energy in CO_2 plasma and (*b*) CO_2 conversion levels as a function of applied voltage on CNFs and plane electrodes, $f = 1$ kHz.

the conversion. For better understanding of the importance of electron impact reactions in CO_2 plasma, Boltzmann equation for electrons was solved using Bolsig+ code [8] and reaction rate coefficients as a function of average electron energy is shown in figure 10(*a*). Cross sections data of one elastic, eight vibrational, two electronic excitation, one ionization and one attachment were used in the simulation at 1 atm. At low electron energies (0–4 eV) rate coefficients of vibrational excitations are much higher. Further increase in the electron energy leads to considerable increase in rate coefficients for dissociative excitations which are responsible mainly for CO_2 decomposition. Figure 10(*b*) shows the conversion enhancement using CNFs electrode at the same measured voltage levels with plane electrodes due to increase in energy deposition and reactive microdischarges. In that sense the number of dissociative electronic excitation channels increases. CNFs can also change the surface chemistry and open new reaction routes on the surface.

4. Conclusions

A microplasma reactor having tungsten oxide nanowires or CNFs as electrodes were fabricated in a barrier discharge configuration. Field enhancement at the apex of the tips of nanostructures resulted in electron emission at atmospheric pressure in air. Decrease in breakdown voltage during the barrier discharge generation resulted in a higher number of microdischarges and higher power deposition at the same measured potential compared with plane cathodes. Reactivity of the discharge can be increased by using CNFs electrode for CO_2 decomposition.

Acknowledgments

This research was supported by the Technology Foundation STW, applied science division of NWO and the technology program of the Ministry of Economic Affairs.

References

[1] Becker K H, Schoenbach K H and Eden J G 2006 *J. Phys. D: Appl. Phys.* **39** R55
[2] Nozaki T, Hattori A and Okazaki K 2004 *Catal. Today* **98** 607
[3] Guillorn M A, Melechko A V, Merkulov V I, Ellis E D, Britton C L, Simpson M L, Lowndes D H and Baylor L R 2001 *Appl. Phys. Lett.* **79** 3506
[4] Zhou J, Gong L, Deng Z, Chen J, She J C, Xu N S, Yang R and Wang Z L 2005 *Appl. Phys. Lett.* **87** 223108
[5] Park S J and Eden J G 2004 *Appl. Phys. Lett.* **84** 4481
[6] Tas M A 1995 Plasma induced catalysis *PhD Thesis* Technical University of Eindhoven p 14
[7] Jani M A, Takaki K and Fujiwara T 1999 *J. Phys. D: Appl. Phys.* **32** 2560
[8] Hagelaar G J M and Pitchford L C 2005 *Plasma Sources Sci. Technol.* **14** 722